Proceedings of the Symposium on Colossal Magnetoresistance

Ellipsometric Studies of $NdMnO_3$ Single Crystals

G.J. Babonas[a], A. Reza[a], R. Szymczak[b], M. Baran[b], S. Shiryaev[c], J. Fink-Finowicki[b] and H. Szymczak[b,*]

[a]Semiconductor Physics Institute, Goštauto 11, 2600 Vilnius, Lithuania
[b]Institute of Physics, Polish Academy of Sciences
al. Lotników 32/46, 02-668 Warsaw, Poland
[c]Institute of Solid State and Semiconductors Physics, NAS
P. Brovka Street, 220072, Minsk, Belarus

Ellipsometric studies of $NdMnO_3$ single crystals of orthorhombic symmetry were carried out in the spectral range 0.5–5.0 eV. Experimental data, which were obtained on the $(001)_{pc}$-type planes of pseudo-cubic system, were analyzed in the model of biaxial crystal. For the first time, three components ε_x, ε_y, ε_z of the effective dielectric function for manganites of orthorhombic symmetry were determined. From ellipsometric data, the spectra of optical conductivity and loss function were also calculated and considered. The fine structure of the spectra and optical anisotropy was the basis for discussion of the microscopic origin of the optical transitions responsible for the optical features. The electronic excitations due to dipole-forbidden spin-allowed transitions of the $d-d$-type in Mn-ions, $f-f$-type in Nd-ions and charge-transfer $2p(\mathrm{O})-3d(\mathrm{Mn})$ transitions were taken into account. The data for $NdMnO_3$ were compared with those obtained for other related undoped and doped single crystals of perovskite-type structure, $LaMnO_3$, $(LaBa)(MnCo)O_3$ and $(LaCa)CoO_3$.

PACS numbers: 71.20.–b, 78.20.Ci

1. Introduction

Undoped $RMnO_3$ (R = La, Nd, Pr) and doped $R_{1-x}A_xMnO_3$ (A = Ca, Sr, Ba) manganites have attracted a lot of attention due to their colossal magnetoresistance [1]. The double exchange model was used to explain the ferromagnetism

*corresponding author; e-mail: szymh@ifpan.edu.pl

and metallicity of manganites. In order to interpret the colossal magnetoresistance, two additional models were developed, which have taken into account the polarons due to the Jahn–Teller effect for Mn^{3+} ions and the orbital fluctuations. In order to investigate the microscopic mechanism of these phenomena, the optical properties of manganites were studied along with the magnetic interactions. The studies of optical response were used to probe the orbital and spin ordering in $LaMnO_3$ [2], heavily doped $Nd_{1-x}Sr_xMnO_3$ [3], $Pr_{1-x}Ca_xMnO_3$ [4], $Bi_{1-x}Ca_xMnO_3$ [5] and layered manganite $La_{1/2}Sr_{3/2}MnO_4$ [6]. The orbital correlation was found to exist far above the Néel temperature T_N in $Nd_{1-x}Sr_xMnO_3$ [3]. The nanoscale phase separation was revealed in $La_{0.7}Ca_{0.3}MnO_3$ films [7, 8] leading to the texture-driven optical anisotropy of the optical response. Studies of compositional and temperature dependence in $La_{1-x}Ca_xMnO_3$ have also shown [9] that short-range charge ordering fluctuations are anomalously strong in manganites.

The fine structure of optical spectra of manganites was also the object of wide discussions. In general, the excitations of free and bound electrons were taken into account. The Drude-term-like contribution of free charge carriers was distinguished in thin films of doped manganites $La_{0.7}Ca_{0.3}MnO_3$ [7, 10], $La_{0.7}Sr_{0.3}MnO_3$, $Nd_{0.7}Sr_{0.3}MnO_3$ [10] and $Pr_{0.8}Sr_{0.2}MnO_3$ [11] whereas no pronounced response of this type was noticed even in the metal-like region for polycrystalline $La_{7/8}Sr_{1/8}MnO_3$ [12] and $La_{1.2}(Sr_{1.8-x}Ca_x)Mn_2O_7$ [13] samples. In $Pr_{1/2}Sr_{1/2}MnO_3$ a spectral weight was transferred from high- to low-energy photon region with increase in the Drude-like peak as the magnetic field was increased up to 14 T [14]. Similar temperature and magnetic field dependent transfer of the spectral weight was observed in cation-deficient $La_{0.936}Mn_{0.982}O_3$ single crystal [15].

It should be noted that the studies of optical reflectivity spectra from cleaved and polished surfaces of $La_{1-x}Sr_xMnO_3$ single crystals have shown [16] that a small Drude-type contribution can be due to a deterioration of the sample surface, in particular for heavily doped crystals. The spectral weight of the Drude-like peak increased dramatically by annealing the $La_{1-x}Ca_xMnO_3$ ($x = 0.1$, 0.265) single crystals [17].

The excitation of bound electrons results in an appearance of more or less pronounced optical features in the spectra of manganites. The absorption spectra of $Pr_{0.8}Sr_{0.2}MnO_3$ thin films were decomposed into the regions of indirect (2.0–2.4 eV) and direct (3.2–3.5 eV) optical transitions with the energy gaps varying with the grain size [11]. As a rule, some distinct peaks were observed in the optical spectra of manganites [1] which were usually approximated by the Lorentzian-type lines. The strong peaks were interpreted by charge transfer $2p(O)-3d(Mn)$ and intraconfigurational $d-d$ (Mn^{3+}) transitions. It should be noted that the microscopic mechanism of the optical transitions responsible for the optical features in the spectra of manganites is not completely understood. Therefore, the optical studies of various manganites are of a particular importance for revealing of general regularities in their electronic structure.

In the present work the ellipsometric studies of $NdMnO_3$ single crystals were carried out. For the first time, all the components of the effective dielectric function for manganites of orthorhombic symmetry were determined for the samples of distorted pseudo-cubic perovskite structure. The analysis of the fine structure and optical anisotropy of the spectra was the basis for the discussion of the microscopic origin of the optical transitions responsible for the optical features. The data for $NdMnO_3$ were compared with those obtained for other perovskites, $LaMnO_3$, $(LaBa)(MnCo)O_3$, and $(LaCa)CoO_3$.

2. Experimental

Single crystals of $NdMnO_3$ were grown by electrodeposition technique (for details, see [18] and references therein). X-ray diffraction has shown that the samples were characterized by the space group *Pbnm* of orthorhombic symmetry with the lattice constants $a = 0.5405$ nm, $b = 0.5743$ nm, $c = 0.7566$ nm. The latter values are close to those determined previously [19] for $NdMnO_3$. From the analysis of cation composition [18] it follows that 2–3% of Mn-sites are occupied by Mn^{4+} leading to approximately 1% excess oxygen in $NdMnO_{3.01}$. The samples possessed natural $(100)_{pc}$-type perovskite pseudo-cubic faces from which the optical measurements were performed. As is known [20], in manganites the growth axis is close to $\langle 100 \rangle_{pc}$ direction of the pseudo-cubic cell.

The structure of $NdMnO_3$ (Fig. 1) may be viewed as the distorted perovskite-type lattice composed of Mn–O polyhedra sharing apical O-atoms. In order to estimate the interatomic distances in $NdMnO_3$, we have used the atom positions

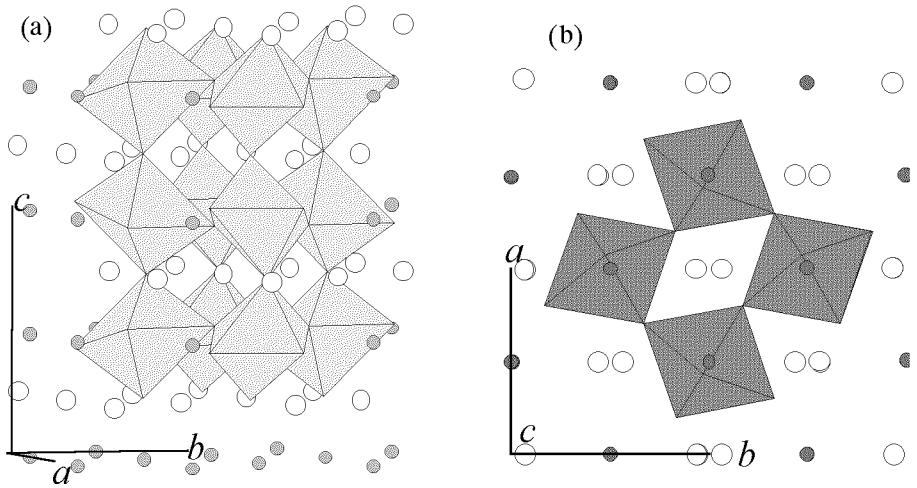

Fig. 1. Structure of orthorhombic $NdMnO_3$ (space group *Pbnm*) as composed by Mn–O octahedra and viewed along the direction close to *a*-axis (a) and *c*-axis (b). The atoms shown are Mn (small circles) and Nd (larger circles).

determined in [19] and the values of lattice constants for investigated samples. The Mn–O octahedron is composed of the nearest O atoms at distances 0.192 and 0.222 nm in the *ab* plane of orthorhombic lattice and two apical O atoms along the *c*-axis at 0.193 nm from Mn atom. The shortest Mn–Mn distance in the *ab* plane is 0.394 nm while it is equal to $c/2 = 0.379$ nm along the *c*-axis with the angle $\approx 156°$ between bonds Mn–O–Mn.

The magnetic characteristic of orthorhombic $NdMnO_3$ crystal was obtained by measuring the temperature (5–300 K) and field (up to 5 T) dependence that has been determined in magnetic field applied along the crystallographic axes (a, b, c). At $T_N \approx 78$ K a transition associated with the ordering of the Mn^{3+} from paramagnetic state to some kind of noncollinear antiferromagnetic (AF) state was found in agreement with reference data [21, 22]. A strong magnetic anisotropy was observed with the easy *c*-axis of ferromagnetic component and practically isotropic *ab* plane. At ≈ 40 K some transformation of AF structure appeared most probably due to a change of canting angle [23]. Below 20 K the evidence of AF ordering of Nd^{3+} ions was found.

Some other manganites were also studied in order to compare the optical data obtained for $NdMnO_3$. The structure of $LaMnO_3$ samples [18], which have been also grown by the electrodeposition technique, was similar as that for $NdMnO_3$. The orthorhombic symmetry was found for the space group $Pbnm$ and lattice parameters $a = 0.5493$ nm, $b = 0.5536$ nm, $c = 0.7821$ nm. The $(La_{0.74}Ba_{0.26})(Mn_{0.8}Co_{0.2})O_3$ single crystal grown from flux melt [24] was characterized by a pseudo-cubic crystal structure ($a_{pc} = 0.390$ nm) with small rhombohedral distortion (space group $R\bar{3}c$) at 300 K. The single crystal of $(La_{0.9}Ca_{0.1})CoO_3$ was grown by a floating zone technique and was characterized by trigonal symmetry (space group $R\bar{3}m$ with lattice constants $a = 0.54395$ nm, $c = 1.30953$ nm in hexagonal system settings). Twinning structure similar to that in $La_{1-x}Sr_xCoO_3$ [20] was observed in the investigated $(LaCa)CoO_3$ sample.

In this work the optical properties of perovskite-type samples were considered in the pseudo-cubic system. For this reason and due additional possible influence of twinning effects [20], the pseudodielectric function approximation [25] was mostly used in the interpretation of the optical response. In this approximation the experimental data were treated in the model of isotropic crystal taking into account that the main contribution to the optical response came from the dielectric function tensor projection onto the intersecting line between the sample surface and plane of light incidence [25]. The optical anisotropy in the $(100)_{pc}$-type planes of pseudo-cubic perovskite $NdMnO_3$ sample was assumed to characterize the basic features of orthorhombic or trigonal lattice in the case of $(LaCa)CoO_3$. In the pseudo-cubic perovskite system (x, y, z) with i-axis normal to the sample surface and j-axis in the plane of light incidence, the effective dielectric function components ε_x, ε_y, ε_z were determined for $NdMnO_3$ as for biaxial crystal [26] from the Fresnel coefficients for light polarized parallel (p) or perpendicular (s) to

the plane of light incidence

$$r_{\mathrm{p}} = \frac{\sqrt{\varepsilon_i}\sqrt{\varepsilon_j}\cos\varphi - \left(\varepsilon_i - \sin^2\varphi\right)^{1/2}}{\sqrt{\varepsilon_i}\sqrt{\varepsilon_j}\cos\varphi + \left(\varepsilon_i - \sin^2\varphi\right)^{1/2}}, \tag{1}$$

$$r_{\mathrm{s}} = \frac{\cos\varphi - \left(\varepsilon_k - \sin^2\varphi\right)^{1/2}}{\cos\varphi + \left(\varepsilon_k - \sin^2\varphi\right)^{1/2}}, \tag{2}$$

where $i,\ j,\ k = x,\ y,\ z,\ i \neq j \neq k \neq i$ and φ is the angle of light incidence. It should be noted that twinning structure typical of the samples grown by floating zone technique [27] was absent in the investigated $NdMnO_3$ sample.

The ratio ρ of the complex amplitude reflection coefficients

$$\rho = \frac{r_{\mathrm{p}}}{r_{\mathrm{s}}} = \tan\Psi\exp(\mathrm{i}\Delta), \tag{3}$$

where $\Psi,\ \Delta$ are ellipsometric parameters, was determined from ellipsometric measurements at 300 K in the spectral region 0.5–5.0 eV. The photometric ellipsometer [28] with rotating analyzer was used and the signal was processed on-line by a non-linear regression analysis. The experiments were performed at $\varphi = 70°$.

In the pseudodielectric function approximation, $\langle\varepsilon_i\rangle$ $(i = x,\ y,\ z)$ spectra were calculated from p-values (3):

$$\langle\varepsilon_i\rangle = \left[\left(\frac{1-\rho_i}{1+\rho_i}\right)^2\tan^2\varphi + 1\right]\sin^2\varphi, \tag{4}$$

where i-axis was parallel to the plane of light incidence.

3. Results and discussion

Figure 2 shows the spectra of ellipsometric parameters measured from the $(010)_{\mathrm{pc}}$ plane of $NdMnO_3$ sample. The spectra indicate two main optical features in the region 1–2 and 3–4 eV as in the other manganite-type compounds [1]. In addition to the broad features, a series of narrower lines was observed in the region 2–3 eV (Fig. 3). In this range the spectra of the complex pseudodielectric function $\langle\varepsilon\rangle$ were described by the contributions of Lorentzian-like terms

$$\varepsilon(E) = \varepsilon_0 + \sum_j \frac{A_j}{E_j^2 - E^2 - \mathrm{i}E\Gamma_j}, \tag{5}$$

where $A_j,\ E_j$, and Γ_j is the amplitude, energy, and halfwidth of j-th line and ε_0 is the contribution of other optical transitions outside the spectral range under consideration. The fitting procedure has shown two strongest lines at 2.33 and 2.69 eV with halfwidth 0.16 and 0.23 eV, respectively. These lines were correlated to the intraconfigurational $f-f$ transitions in Nd^{3+} ions from the ground state $^4I_{9/2}$ to the excited states $^4G_{7/2}$ and $^2G_{9/2}$ [29]. The $f-f$-type transitions $^4I_{15/2} \rightarrow {}^4I_{11/2},\ {}^4I_{9/2}$, in Er^{3+} ions were observed in hexagonal manganite $ErMnO_3$ [30].

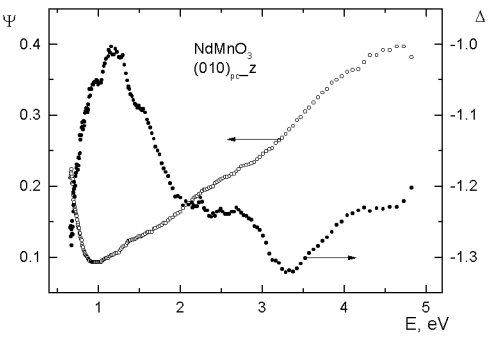

Fig. 2. Spectral dependence of ellipsometric parameters Ψ and Δ measured from the $(010)_{\rm pc}$ plane of $NdMnO_3$ sample with the z-axis parallel to the plane of light incidence.

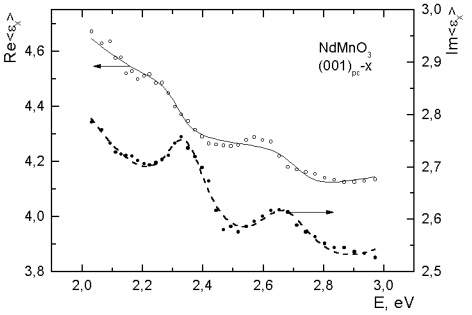

Fig. 3. Experimental (points) and fitted by Lorentzian lines (curves) spectra of pseudodielectric function determined from ellipsometric measurements on $(001)_{\rm pc}$ plane of $NdMnO_3$ sample with x-axis in the plane of light incidence in the region of $^4I_{9/2} \rightarrow {}^4G_{7/2}$, $^2G_{9/2}$ transition in Nd^{3+} ions.

The ellipsometric data $\Psi(E)$, $\Delta(E)$ obtained from the planes $(010)_{\rm pc}$ and $(100)_{\rm pc}$ with x, z, and y axes, respectively, aligned parallel to the plane of light incidence were used to determine the effective dielectric function components ε_x, ε_y, ε_z for $NdMnO_3$ (Fig. 4) by solving the inverse problem according to (1)–(3). The fine structure of experimental spectra was fitted by the Lorentzian-type contributions (5). As is seen from Fig. 4, three main structures labelled A, B, C are observed. The main peak C at $E_C = 3.67$ eV is quite strong for all polarizations. The analogous optical feature was observed in $La_{1-x}Sr_xMnO_3$ ($0 < x < 0.3$) [31, 32] and was found to shift to the lower photon energy at an increase in Sr-content and increasing the temperature from 10 to 300 K in $Nd_{0.7}Sr_{0.3}MnO_3$ [10]. In $NdMnO_3$ the energy of the peak B depends slightly on light polarization and equals to 2.06, 1.9, and 2.36 eV for ε_x, ε_y, and ε_z components, respectively. The B-peak amplitude is significantly lower for ε_z-component though the oscillator strength is high enough indicating that the other optical transitions occur in this spectral range. A similar optical anisotropy was observed in $LaMnO_3$ [2]: the optical conductivity

$\sigma(E)$ peak at ≈ 2 eV was more pronounced for polarization $e \parallel ab$ than for $e \parallel c$ for the setting of orthorhombic axes a, b, c (in the notations of space group $Pbnm$). In insulating $Sm_{0.6}Sr_{0.4}MnO_3$ [33] and $Pr_{0.6}Ca_{0.4}MnO_3$ [4] the peak, which was analogous to peak B in $NdMnO_3$, increased at lowering the temperature below the charge-ordered state ($T_{CO} \approx 235$ K). A similar temperature behavior was observed in doped manganites $(Nd_{0.5}Sr_{0.5})MnO_3$, $(La_{0.5}Nd_{0.5})_{0.6}Sr_{0.4}MnO_3$, $(Nd_{1-x}Sm_x)_{0.6}Sr_{0.4}MnO_3$ ($x = 0.5, 0.75$) [33] below the insulator–metal transition temperature though the fine structure was masked by intraband free charge carrier transitions, which caused the spectral weight transfer to the Drude-type band at low temperatures. The peak A manifests itself as a bump on the lower-energy side of a stronger peak B. Peak A is better resolved for the ε_z-component (Fig. 4c).

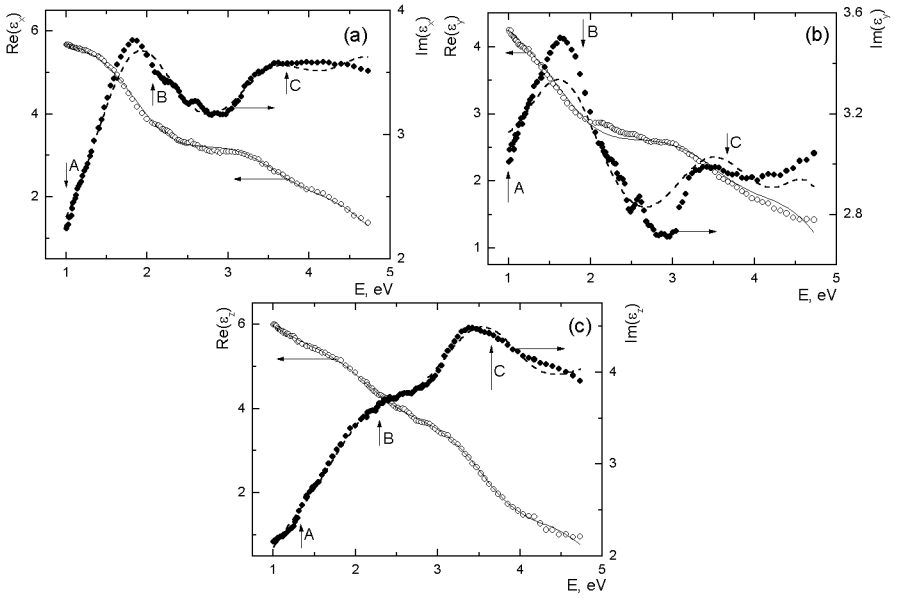

Fig. 4. Experimental (points) and fitted by Lorentzian lines (curves) spectra of the effective dielectric function components ε_x (a), ε_y (b), ε_z (c) for $NdMnO_3$.

Figure 5 shows the spectra of optical conductivity $\langle\sigma\rangle(E)$ and loss function $-\mathrm{Im}(1/\langle\varepsilon\rangle)$ calculated from pseudodielectric function obtained from ellipsometric measurements on the $(010)_{pc}$ and $(100)_{pc}$ planes of $NdMnO_3$. Numerical σ-values at peaks B and C in $NdMnO_3$ are close to those for $(LaSr)MnO_3$ [31, 32]. In both optical conductivity and loss function spectra the optical anisotropy is clearly seen. In the optical conductivity spectra the $\langle\sigma\rangle_x$ and $\langle\sigma\rangle_y$ components are quite close though some difference occurs at $E < 1.7$ eV. In the loss function spectra the x- and y-components show similar spectral dependence though differ in magnitude. A strong increase in loss function should be noted at $E < 1$ eV for z-component.

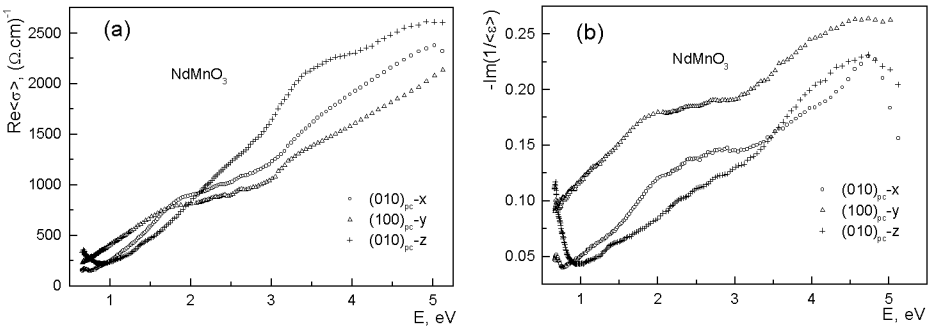

Fig. 5. Optical conductivity (a) and loss function (b) spectra of $NdMnO_3$ calculated from pseudodielectric function determined by ellipsometric measurements from pseudocubic planes (010) and (100) with axes x, z, and y, respectively, in the plane of light incidence.

The optical anisotropy is well illustrated by anisotropy parameter

$$\Delta_{ij} = \frac{\varepsilon_i'' - \varepsilon_j''}{\sqrt{\varepsilon_i''^2 + \varepsilon_j''^2}}, \tag{6}$$

where ε_k'' is the k-th component of the imaginary part of dielectric function. Figure 6 presents the $\Delta_{ij}(E)$ spectra for the effective dielectric function of $NdMnO_3$ shown in Fig. 4. As is seen, the in-plane optical anisotropy Δ_{xy} differs considerably from Δ_{xz} and Δ_{yz} with respect to the z-axis. In the whole spectral range the optical anisotropy with respect to the z-axis is quite large though it changes the sign at $E \approx 2$ eV. In a higher photon energy region Δ_{xz} and Δ_{yz} show similar spectral dependence and the in-plane anisotropy does not depend on the photon energy. However, at $E < 1.7$ eV the in-plane anisotropy is significant and varies with photon energy.

Figure 7 presents a comparison of the dielectric function for $NdMnO_3$ and some other investigated related perovskite-type compounds. As is seen, similar optical features manifest themselves in all the spectra though some transformation should be noticed. In the low energy region the optical response is increased for doped single crystals $(LaCa)CoO_3$ and $(LaBa)(MnCo)O_3$ most probably due to enhanced contribution of free charge carriers. This contribution masks the peaks A and B. The fine structure of pseudodielectric function $\langle\varepsilon\rangle$ spectra for $LaMnO_3$ was qualitatively similar to that for $NdMnO_3$. However, in $LaMnO_3$ the optical anisotropy was not observed in the ellipsometric spectra obtained from $(100)_{\rm pc}$-type planes. The analysis of the fine structure in $\langle\varepsilon\rangle(E)$ of $LaMnO_3$ revealed the doublet-type structure of peak C ($E_{C1} = 3.72$ eV, $E_{C2} = 4.54$ eV). Thus, the $\langle\varepsilon\rangle(E)$ spectra in the region of higher photon energy are similar for $NdMnO_3$ and $LaMnO_3$. However, in $LaMnO_3$ the peak B occurs at lower energy ($E_B = 1.47$ eV) than in $NdMnO_3$. The optical response measured from the $(111)_{\rm pc}$

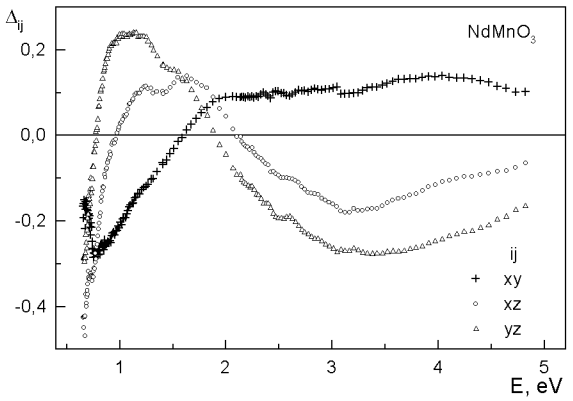

Fig. 6. Spectral dependence of anisotropy parameter for the components of effective dielectric function in $NdMnO_3$.

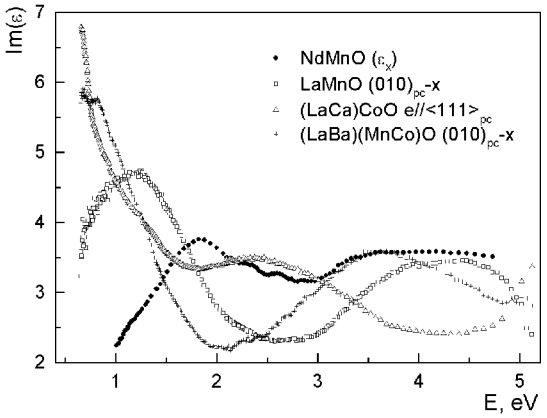

Fig. 7. Imaginary part of the dielectric function for investigated perovskite-type single crystals.

plane of $LaMnO_3$ was weaker than that from $(010)_{pc}$ and a lower energy peak at $E_A \approx 0.8$ eV could be distinguished as it was in the case of $NdMnO_3$.

In the $\langle\varepsilon\rangle(E)$ spectra of (LaCa)CoO_3 crystal (Fig. 7) the peak at 2.5 eV should be most probably correlated to the peak C in $NdMnO_3$ and $LaMnO_3$ indicating the shift of charge transfer transitions in cobaltites and manganites [34]. The bump at ≈ 1.4 eV in the $\langle\varepsilon\rangle(E)$ spectra of (LaCa)CoO_3 is in a good agreement with the low energy peak at ≈ 1.3 eV observed in $LaCoO_3$ [35]. In addition, an increase in optical response in the investigated doped $(La_{0.9}Ca_{0.1})CoO_3$ sample agrees well with a similar dependence of the optical conductivity spectra in $La_{1-x}Sr_xCoO_3$ at an increase in Sr-content [35]. It should be noted that the optical anisotropy was weak in investigated (LaCa)CoO_3 sample most probably because of a twinning structure observed under polarizing microscope.

The observed regularities in the dielectric function spectra can be interpreted as follows. As in $La_{1-x}Sr_xMnO_3$ [31, 32], in $NdMnO_3$ the peaks B and C can be attributed to the charge transfer excitations from the O $2p$ to the Mn $3d$ states, correspondingly to the transitions $t_{2g}^3e_g^1 \rightarrow t_{2g}^3e_g^2L$ and $t_{2g}^3e_g^1 \rightarrow t_{2g}^4e_g^1L$, where L is a ligand hole. In the spectral range 0.5–2.5 eV some contribution can be also due to the d–d-type transitions in Mn ions. The polarized intersite transitions of d-electrons from Mn^{3+} to Mn^{4+} observed in $Pr_{0.6}Ca_{0.4}MnO_3$ [4] can be important in $NdMnO_3$ as well. The in-plane optical anisotropy observed in $NdMnO_3$ (Fig. 6) can be related to some charge ordering in the system of Mn^{3+} and Mn^{4+} ions. On the basis of experimental investigations of nonlinear optical spectroscopy (second harmonic generation and Faraday effect), broad bands at 1.7 and 2.7 eV were assigned to the d–d transitions between Mn^{3+} levels in hexagonal manganites $YMnO_3$ and $ErMnO_3$. Recent theoretical calculations of the energy level structure by a cluster approximation (MnO_6-octahedron) in $LaMnO_3$ has shown [36] a great number of dipole-allowed one-electron charge transfer transitions from oxygen $t_{1u}(\sigma)$-, $t_{1u}(\pi)$-, $t_{2u}(\pi)$-orbitals to e_g- and t_{2g}-states of $3d$ (Mn) in the spectral range 2.5–11 eV and a series of dipole-forbidden transitions. The lowest energy dipole-forbidden transition $t_{1g}(\pi) \rightarrow e_g$ was found at 1.7 eV which was followed by a weak dipole-allowed transition $t_{2u}(\pi) \rightarrow e_g$ at 2.5 eV and strong dipole-allowed $t_{1u}(\pi) \rightarrow e_g$ transition at 3.5 eV.

Summarizing, the regularities in the dielectric function spectra of investigated related compounds of perovskite-type structure have shown, on the one hand, that the higher energy peak C depends significantly on the transition metal type. A replacement of Mn by Co results in a large shift of the peak towards lower photon energies. On the other hand, the type of rare-earth (RE) element influences mainly on the low-energy peaks A and B. A doping of perovskites substituting trivalent RE elements by divalent elements Ca and Ba leads to an increase in Drude-type contribution indicating explicitly an increase in free charge carriers. The present study has also shown that the optical anisotropy can provide additional arguments for the interpretation of optical transitions in perovskite-type compounds.

Acknowledgments

The work in Warsaw was partly supported by the State Committee for Scientific Research (Poland) under the project 5P03B01620. The authors acknowledge also the technical assistance of Mrs. B. Krzymanska.

References

[1] J.M.D. Coey, M. Viret, S. von Molnar, *Adv. Phys.* **48,** 167 (1999).

[2] K. Tobe, T. Kimura, Y. Okimoto, Y. Tokura, *Phys. Rev. B* **64,** 184421 (2001).

[3] K. Tobe, T. Kimura, Y. Tokura, *Phys. Rev. B* **67,** 140402(R) (2003).

[4] Y. Okimoto, Y. Tomioka, Y. Onose, Y. Otsuka, Y. Tokura, *Phys. Rev. B* **57,** R9377 (1998).

[5] H.L. Liu, S.L. Cooper, S.-W. Cheong, *Phys. Rev. Lett.* **81,** 4684 (1998).

[6] T. Ishikawa, K. Ookura, Y. Tokura, *Phys. Rev. B* **59,** 8367 (1999).

[7] R. Rauer, J. Bäckström, D. Budelmann, M. Kurtfiß, M. Schilling, M. Rübhausen, T. Walter, K. Dörr, S.L. Cooper, *Appl. Phys. Lett.* **81,** 3777 (2002).

[8] A.S. Moskvin, E.V. Zenkov, Yu.P. Sukhorukov, E.V. Mostovshchikova, N.N. Loshkareva, A.R. Kaul, O.Yu. Gorbenko, *J. Phys., Condens. Matter* **15,** 2635 (2003).

[9] K.H. Kim, S. Lee, T.W. Noh, S.-W. Cheong, *Phys. Rev. Lett.* **88,** 167204 (2002).

[10] M. Quijada, J. Černe, J.R. Simpson, H.D. Drew, K.H. Ahn, A.J. Millis, R. Shreekala, R. Ramesh, M. Rajeswari, T. Vanekatesan, *Phys. Rev. B* **58,** 16093 (1998).

[11] T. Suzuki, P. Jasinki, V. Petrovsky, X.-D. Zhou, H.U. Anderson, *J. Appl. Phys.* **93,** 6223 (2003).

[12] J.H. Jung, K.H. Kim, H.J. Lee, J.S. Ahn, N.J. Hur, T.W. Noh, M.S. Kim, J.-G. Park, *Phys. Rev. B* **59,** 3793 (1999).

[13] H.L. Liu, J.L. Her, C.H. Shen, R.S. Liu, *J. Appl. Phys.* **93,** 6894 (2003).

[14] J.H. Jung, H.J. Lee, T.W. Noh, Y. Moritomo, Y.J. Wang, X. Wei, *Phys. Rev. B* **62,** 8634 (2000).

[15] V. Golovanov, L. Mihaly, C.O. Homes, W.H. McCarroll, K.V. Ramanujachary, M. Greenblatt, *Phys. Rev. B* **59,** 153 (1999).

[16] K. Takenaka, K. Iida, Y. Sawaki, S. Sugai, Y. Moritomo, A. Nakamura, *J. Phys. Soc. Jpn.* **68,** 1828 (1999).

[17] O.R. Mercier, R.G. Buckley, A. Bittar, H.J. Trodahl, E.M. Haines, J.B. Metson, Y. Tomioka, *Phys. Rev. B* **64,** 035106 (2001).

[18] S.N. Barilo, V.I. Gastal'skaya, S.V. Shiryaev, G.L. Bychkov, L.A. Kurochkin, S.N. Ustinovich, R. Szymczak, M. Baran, B. Krzymanska, *Fiz. Tverd. Tela* **45,** 139 (2003).

[19] S. Quezel-Ambrunaz, *Bull. Soc. Franc. Mineral. Cristallogr.* **91,** 339 (1968).

[20] T. Matsuura, J. Mizusaki, S. Yamauchi, K. Fueki, *Jpn. J. Appl. Phys.* **23,** 1197 (1984).

[21] A. Muñoz, J.A. Alonso, M.J. Martinez-Lope, J.L. García-Muñoz, M.T. Fernández-Díaz, *J. Phys., Condens. Matter* **12,** 1361 (2000).

[22] A.A. Mukhin, V.Yu. Ivanov, V.D. Travkin, A.M. Balbashov, *J. Magn. Magn. Mater.* **226-230,** 1139 (2001).

[23] S.Y. Wu, C.M. Kuo, H.Y. Wang, W.-H. Li, K.C. Lee, J.W. Lynn, R.S. Liu, *J. Appl. Phys.* **87,** 5822 (2000).

[24] D.D. Khalyavin, M. Pekala, G.L. Bychkov, S.V. Shiryaev, S.N. Barilo, I.O. Troyanchuk, J. Mucha, H. Misiorek, R. Szymczak, M. Baran, H. Szymczak, *J. Phys., Condens. Matter* **15,** 925 (2003).

[25] D.E. Aspnes, *J. Opt. Soc. Am.* **70,** 1275 (1980).

[26] G.-J. Babonas, L. Leonyuk, V. Maltsev, R. Szymczak, A. Reza, M. Baran, L. Dapkus, *Acta Phys. Pol. A* **100,** 553 (2001).

[27] M. Dechamps, A.M. de Leon Guevara, L. Pinsard, A. Revcolevschi, *Philos. Mag. A* **80,** 119 (2000).

[28] G.-J. Babonas, A. Reza, V. Maltsev, A. Galickas, L. Dapkus, *Lith. J. Phys.* **42,** 161 (2002).

[29] G.H. Dieke, *Spectra and Energy Levels of Rare Earth Ions in Crystals*, Wiley, New York 1968, p. 401.

[30] C. Degenhardt, M. Fiebig, D. Fröhlich, Th. Lottermoser, R.V. Pisarev, *Appl. Phys. B* **73,** 139 (2001).

[31] S. Yamaguchi, Y. Okimoto, K. Ishibashi, Y. Tokura, *Phys. Rev. B* **58,** 6862 (1998).

[32] K. Takenaka, K. Iida, Y. Sawaki, S. Sugai, Y. Morimoto, A. Nakamura, *J. Phys. Soc. Jpn.* **68,** 1828 (1999).

[33] A. Machida, Y. Morimoto, A. Nakamura, *Phys. Rev. B* **58,** 12540 (1998).

[34] T. Arima, Y. Tokura, *J. Phys. Soc. Jpn.* **64,** 2488 (1995).

[35] Y. Tokura, Y. Okimoto, S. Yamaguchi, H. Taniguchi, T. Kimura, H. Takagi, *Phys. Rev. B* **58,** R1699 (1998).

[36] Yu.P. Sukhorukov, N.N. Loshkareva, E.A. Gan'shina, E.V. Mostovshchikova, I.K. Rodin, A.R. Kaul, O.Yu. Gorbenko, A.A. Bosak, A.S. Moskvin, E.V. Zvenkov, *Zh. Eksp. Teor. Fiz.* **123,** 293 (2003).